Rothmund-Thomson syndrome-like RECQL4 truncating mutations cause a haploinsufficient low-bone-mass phenotype in mice

Castillo-Tandazo, Wilson, Frazier, Ann E., Sims, Natalie A., Smeets, Monique F. and Walkley, Carl R.

Castillo-Tandazo, W., Frazier, A. E., Sims, N. A., Smeets, M. F. and Walkley, C. R. (2021). Rothmund-Thomson syndrome-like RECQL4 truncating mutations cause a haploinsufficient low-bone-mass phenotype in mice. *Molecular and Cellular Biology*, 41(3), pp. Article e00590-20. https://doi.org/10.1128/MCB.00590-20

MCB Accepted Manuscript Posted Online 23 December 2020
Mol Cell Biol doi:10.1128/MCB.00590-20

Rothmund-Thomson Syndrome-like RECQL4 truncating mutations cause a haploinsufficient low bone mass phenotype in mice

Wilson Castillo-Tandazo[1,2], Ann E Frazier[3,4], Natalie A Sims[1,2], Monique F Smeets[1,2,*] & Carl R Walkley[1,2,5,*]

[1]St. Vincent's Institute of Medical Research, Fitzroy, VIC 3065 Australia;
[2]Department of Medicine, St. Vincent's Hospital, The University of Melbourne, Fitzroy, VIC 3065 Australia;
[3]Murdoch Children's Research Institute, Royal Children's Hospital, Parkville, VIC 3052 Australia.
[4]Department of Paediatrics, University of Melbourne, Parkville, VIC 3052 Australia.
[5]Mary MacKillop Institute for Health Research, Australian Catholic University, Melbourne, VIC, 3000, Australia.

*Contributed equally to this work

Correspondence should be addressed to:
Carl Walkley or Monique Smeets
St. Vincent's Institute
9 Princes St.
Fitzroy 3065 VIC
Australia
T: +61-3-9231-2480
Email: cwalkley@svi.edu.au; msmeets@svi.edu.au

ORCID Identifiers:
Wilson Castillo-Tandazo: 0000-0002-3202-8185
Ann Frazier: 0000-0002-6491-3437
Natalie Sims: 0000-0003-1421-8468
Monique Smeets: 0000-0001-6027-4108
Carl Walkley: 0000-0002-4784-9031

Running Title: RTS-like RECQL4 mutations cause low bone mass.

Keywords: Rothmund-Thomson Syndrome; RECQL4; RecQ; osteoporosis; osteosarcoma; mouse models.
Abstract: 200
Number of Figures: 5

Conflict of Interest Statement: All authors declare no conflicts of interest.

Abstract

Rothmund-Thomson Syndrome (RTS) is an autosomal recessive disorder characterized by defects in the skeletal system such as bone hypoplasia, short stature, low bone mass, and an increased incidence of osteosarcoma. RTS type 2 patients have germline compound bi-allelic protein-truncating mutations of *RECQL4*. As existing murine models employ *Recql4* null alleles, we have attempted to more accurately model RTS by generating mice with patient-mimicking truncating *Recql4* mutations. Truncating mutations impaired the stability and subcellular localization of RECQL4, and resulted in homozygous embryonic lethality and a haploinsufficient low bone mass phenotype. Combination of a truncating mutation with a conditional *Recql4* null allele demonstrated that the skeletal defects were intrinsic to the osteoblast lineage. However, the truncating mutations did not promote tumorigenesis. We utilized murine *Recql4* null cells to assess the impact of human *RECQL4* mutations using an *in vitro* complementation assay. While some mutations created unstable protein products, others altered subcellular localization of the protein. Interestingly, the severity of the phenotypes correlated with the extent of protein truncation. Collectively, our results reveal that truncating RECQL4 mutations in mice lead to an osteoporosis-like phenotype through defects in early osteoblast progenitors and identify RECQL4 gene dosage as a novel regulator of bone mass.

68 **Introduction**

69 Rothmund-Thomson syndrome (RTS) (OMIM #268400) is a rare autosomal
70 recessive disorder that presents with skin rash (poikiloderma; areas of
71 hypopigmentation, hyperpigmentation, telangiectasias and atrophy of the skin),
72 sparse or absent hair, juvenile cataracts, gastrointestinal and skeletal complications
73 (1, 2). Approximately 75% of patients have skeletal abnormalities, including bone
74 hypoplasia, short stature, polydactyly, and low bone mass (3). Furthermore, this
75 syndrome is frequently associated with osteosarcoma (bone cancer) and other
76 malignancies (1, 2, 4, 5). RTS is classified into two forms: RTS type 1, where
77 patients present with juvenile cataracts and have frequent mutations of *ANAPC1,* but
78 do not have increased incidence of osteosarcoma (6); and RTS type 2, where the
79 majority of patients harbor biallelic mutations of *RECQL4* and have a significantly
80 increased incidence of osteosarcoma (2).

81 *RECQL4* is located on the long arm of chromosome eight (8q24.3) (7). The
82 reported mutational spectrum includes the introduction of early stop codons,
83 frameshift mutations, as well as deletions within numerous short introns (<100 bp)
84 that can impair RNA splicing, resulting in protein truncations and loss-of-function
85 alleles (8). The *RECQL4* gene encodes a protein of 1,208 amino acids (aa) that has
86 three well-characterized domains. The N-terminal region shares sequence homology
87 to the essential yeast DNA replication factor Sld2. In higher eukaryotes, this Sld2-like
88 homology domain is unique to RECQL4 (9, 10). Studies have shown that this region
89 has roles in DNA replication and DNA repair, and that it is critical for viability (11-13).
90 The highly conserved central RecQ helicase domain contains an ATPase core with
91 seven motifs that couple ATP hydrolysis to double-stranded DNA (dsDNA)
92 separation (14). This ATP-dependent helicase activity was presumed to be critical for
93 the function of RECQL4. However, using mice with a knock-in mutation (K525A) that
94 inactivates the ATP-dependent helicase function, we recently reported that
95 homozygous mice displayed normal embryonic development, body weight,

hematopoiesis, B and T cell development, and physiological DNA damage repair (15). Finally, the C-terminal region harbors both the R4ZBD domain, in place of an RQC domain seen in other RecQ helicases, and a small C-terminal domain (CTD; 1117-1208aa) associated with DNA-binding affinity (16). Regarding intracellular localization, RECQL4 is primarily localized in the nucleus but has also been reported in the cytoplasm (17, 18). Its distribution within these compartments, however, depends on the cell type and the phase of the cell cycle (17).

RTS Type 2 patients have a high incidence of skeletal abnormalities and osteosarcoma. In a clinical cohort study evaluating 41 RTS patients, 32% developed osteosarcoma (2). Furthermore, an independent cohort reported that the median age at diagnosis in RTS patients was ten years of age (19). This is significantly younger than the median age of sporadic osteosarcoma, which is sixteen years (20). Importantly, we and others have previously reported that in mice the deletion of *Recql4* in pre-osteoblasts or limb bud progenitors caused shorter bones and reduced bone volume (21, 22). However, neither model developed osteosarcoma, even in combination with *Tp53* deficiency (22). In contrast to these models that generated null alleles, RTS patients predominantly have compound heterozygous *RECQL4* mutations that are predicted to generate truncated protein products (4). More than half of these truncate the protein before or within the helicase domain and result in a substantially increased risk of developing osteosarcoma compared to non-truncating mutations (5). Therefore, it is critical to determine the *in vivo* effects of germline truncating *Recql4* mutations in normal homeostasis and tumor development.

To more faithfully model the RTS-relevant *RECQL4* mutation spectrum beyond existing null alleles, we have generated mice bearing truncating mutations that map closely to those reported in RTS patients (15). Here we show that these truncating mutations affected stability and subcellular localization of RECQL4, which translated to a homozygous developmental lethality and a haploinsufficient low bone mass phenotype through defects in early osteoblast progenitors. Additionally, we

observed that the severity of the defect was related to the degree of the truncation, suggesting that gene dosage is an important determinant of the bone phenotype. However, unlike in RTS type 2 patients, these RECQL4 mutations were not sufficient in isolation to initiate tumorigenesis in mice, even after exposure to irradiation. This would suggest that additional molecular and cellular changes are required for the full spectrum of RTS phenotypes to develop.

Results

Truncating mutations of RECQL4 affect protein expression levels and cause developmental lethality in homozygotes.

To understand the *in vivo* impact of truncating RECQL4 mutations, we generated two novel mouse *Recql4* alleles (15). These new mutations were similar to common mutations seen in RTS type 2 patients (Fig 1A). The p.Gly522GlufsTer43 (G522Efs) mutation, comparable to the human p.Cys525AlafsX33 (C525Afs) mutation, was created by a two-base pair insertion (c.1646_1647insGA). The frameshift caused a premature stop codon 44aa downstream, resulting in a predicted protein of 566aa lacking the majority of the helicase domain and all of the C-terminal domain. The second allele was a p.Arg347* (R347X) mutation, a nonsense mutation (c.1122C>T) identified from an N-ethyl-N-nitrosourea (ENU) mutagenesis collection, similar to p.Arg350GlyfsX21 (R350Gfs) in RTS patients. This mutation yielded a predicted 347aa protein lacking both the helicase and C-terminal domains entirely (Fig 1B). To verify the genotypes of these mice, we used PCR-restriction fragment length polymorphism (PCR-RFLP) for the G522Efs allele, and competitive allele-specific PCR (KASP) assay for the R347X allele, both of which confirmed the correct genotype (S1 Fig).

The heterozygous *Recql4*$^{R347X/+}$ and *Recql4*$^{G522Efs/+}$ mice were viable and fertile. To determine if individual homozygous truncating mutants were viable, the respective heterozygous mice were inbred. We did not recover any *Recql4*$^{R347X/R347X}$ or *Recql4*$^{G522Efs/G522Efs}$ pups at genotyping (day 7-10 after birth), indicating that the homozygous mutants were developmentally lethal (Fig 1C). We have not established the time point in development at which the respective mutants are no longer viable.

Next, we investigated the *in vivo* expression of the predicted truncated proteins. We prepared lysates from the thymus of germline heterozygous mutants of each respective allele and probed them with a monoclonal antibody raised against the first 200aa of murine RECQL4 by Western blot (15). We found a truncated

159 protein product of the predicted size for the R347X mutant in thymocyte extracts,
160 though at a much lower intensity than the WT band (Fig 1D). In contrast, the
161 G522Efs mutant protein could not be detected (Fig 1D), and even when ectopically
162 overexpressed as a cDNA with an N-terminal 3xFlag tag, its expression was
163 significantly lower than the R347X (Fig 1E).

164 To assess whether the truncated proteins had altered cellular localization, we
165 generated N-terminal mCherry-tagged mouse RECQL4 fusion constructs. These
166 were retrovirally infected into the murine osteoblastic Kusa4b10 cell line. Protein
167 localization was analyzed by qualitative fluorescence microscopy. The full-length
168 wild-type murine RECQL4 protein (WT) was predominantly localized in the nucleus
169 as expected, with an apparent enrichment in the nucleolus. The ATP-dependent
170 helicase inactive p.Lys525Ala (K525A) mutation, which we recently reported (15),
171 had a similar localization to WT RECQL4 (Fig 1F). In contrast, the R347X protein,
172 while also localized to the nucleus, was poorly incorporated in the nucleoli (Fig 1F).
173 Interestingly, consistent with the weak protein expression *in vivo* (Fig 1D), the
174 G522Efs protein was poorly expressed and difficult to detect (Fig 1F).

175 We also assessed the cellular localization patterns of similar human RTS
176 associated RECQL4 mutations. For this purpose, we utilized a human N-terminal
177 EGFP-tagged WT, an ATP-helicase inactive K508A mutant, and created the
178 C525Afs and R350Gfs mutations. These constitute the human homologues of, or
179 map closely to, the murine mutations K525A, G522Efs, and R347X, respectively. We
180 found similar qualitative localization results between the human and murine proteins
181 (Fig 1G).

182 Finally, it has been suggested that RECQL4 could localize to the
183 mitochondria (23, 24). Using the fluorescent fusion proteins, we could not detect
184 mouse or human RECQL4 (WT or mutant) in the cytoplasm nor overlapping with the
185 mitochondria (S2 Fig A). To evaluate this result functionally, we assessed
186 mitochondrial function using the Seahorse bioenergetic assay. To enable comparison

of the different point mutations, we used HoxB8 immortalized myeloid progenitor cells (25) derived from *R26*-CreER *Recql4*$^{fl/+}$, *R26*-CreER *Recql4*$^{fl/K525A}$, *R26*-CreER *Recql4*$^{fl/R347X}$, and *R26*-CreER *Recql4*$^{fl/G522Efs}$ and exposed them to tamoxifen for four days to delete the wild-type *Recql4* floxed allele. We found no difference in either basal or maximal oxygen consumption rate (OCR) between the non-tamoxifen and tamoxifen-treated groups (S2 Fig B-E), demonstrating that mutations in RECQL4 that significantly impact protein stability and function do not measurably affect mitochondrial respiration. Taken together, our results demonstrate that the murine RECQL4 mutants behave similarly to their human counterparts; and while the specific mutations impact their level of expression and subcellular localization differently, they do not measurably affect mitochondrial respiration.

Recql4$^{R347X/+}$ and _Recql4_$^{G522Efs/+}$ heterozygosity leads to reduced bone mass phenotype.

We previously reported that complete deletion of *Recql4* in the osteoblast lineage resulted in mice with shorter bones and reduced bone volume (22). RTS patients, however, present with compound heterozygous mutations that result in truncating proteins, rather than null alleles. Therefore, to assess the skeletal/bone phenotypes associated with RTS type 2 relevant RECQL4 mutations, we measured skeletal growth in the two viable heterozygous mutants. We could not evaluate homozygous mutants for either allele due to the developmental lethality previously described. The germline heterozygous animals are therefore most similar to the parents of RTS patients. For all genotypes, ten-week old male mice were analyzed. The heterozygous *Recql4*$^{R347X/+}$ and *Recql4*$^{G522Efs/+}$ mice had a reduced body weight that did not reach statistical significance within the cohort assessed (Fig 2A). We utilized Echo-MRI to investigate a change in fat/lean mass proportion and found no differences (S3 Fig). We then evaluated the tibial length by micro-computed tomography (micro-CT). Overall tibial length in both *Recql4*$^{R347X/+}$ and *Recql4*$^{G522Efs/+}$

mutants was not statistically different compared to either wild-type (littermate) controls or K525A homozygous males (Fig 2B). However, the mediolateral and anteroposterior widths measured by micro-CT in the midshaft tibia were significantly lower in both *Recql4*$^{R347X/+}$ and *Recql4*$^{G522Efs/+}$ mutants, indicating narrower tibiae in both genotypes (Fig 2C and 2D). For comparison, tibiae from the helicase-inactive K525A homozygous mice did not show differences in any of these parameters when compared to the WT controls.

We further looked at possible bone changes in trabecular microarchitecture and cortical morphology of WT and mutant 10-week old male mice. For trabecular analysis, we selected a region corresponding to the secondary spongiosa in the proximal metaphysis of the tibia (Fig 2E). The trabecular bone volume of *Recql4*$^{R347X/+}$ and *Recql4*$^{G522Efs/+}$ mice was significantly lower by 24% and 26%, respectively (Fig 2F). The trabecular number was also lower by 25% in the *Recql4*$^{R347X/+}$ and 20% in the *Recql4*$^{G522Efs/+}$ mice (Fig 2G). The trabecular separation was 25% greater in the *Recql4*$^{R347X/+}$ mice but not different in the *Recql4*$^{G522Efs/+}$ mice (Fig 2H). For cortical analysis, we assessed a region corresponding to the mid-diaphysis of the tibia (Fig 2J). Cortical thickness was 10% lower in the *Recql4*$^{R347X/+}$ mutants, whereas there was a slight (7%) but non-significant decrease in the *Recql4*$^{G522Efs/+}$ mice, compared to controls (Fig 2K). For both the *Recql4*$^{R347X/+}$ and *Recql4*$^{G522Efs/+}$, the periosteal perimeter showed a reduction of 14% and 7%, respectively, when compared with littermate controls (Fig 2L), which was reflected in a lower moment of inertia for both groups (Fig 2M). This suggested a lower torsional rigidity and increased fracture risk in the germline heterozygous truncating mutant mice. In contrast, the non-truncating but ATP-binding helicase-inactive *Recql4*$^{K525A/K525A}$ mutants did not show any change in any trabecular or cortical parameter when compared to the WT control (Fig 2E-2H, 2J-2M). All morphological changes could be visualized in the color-coded 3D reconstructions (Fig 2I and 2N). Additional micro-CT parameters are provided in S4 Fig A-C. Collectively, these

243 results demonstrate that heterozygous truncating mutations of RECQL4 in mice
244 resulted in narrow bones and skeletal dysplasia.

245 Given that several studies have reported RTS patients with hematopoietic
246 defects (26-28) and that there is an established reciprocal relationship between bone
247 and hematopoiesis (29), we assessed whether the changes in skeletal parameters
248 seen in the germline heterozygous mutant mice would impact hematopoiesis.
249 Results showed a decrease in the cell hierarchy involved in myeloid development,
250 which did not affect mature granulocytes or macrophages (S5 Fig). The remaining
251 parameters assessed were normal. Therefore, a single copy of a truncating mutation
252 in the presence of a retained WT allele is not sufficient to cause marked changes in
253 hematopoiesis and is consistent with the reports from RTS patients and the apparent
254 normality of hematopoiesis in their heterozygous parents. Taken together, these
255 observations suggest that heterozygous truncating RECQL4 mutations cause a
256 haploinsufficient low bone mass phenotype similar to that reported in RTS patients.
257 Interestingly, the expression of a single copy of a full-length wild type RECQL4 is
258 sufficient to maintain hematopoiesis, which indicates cellular differences between
259 osteoblast lineage cells and blood-forming cells in sensitivity to *Recql4* gene dosage.
260

261 **Intrinsic defects in osteoblast lineage cells cause the low bone mass**
262 **phenotype of RECQL4 truncating mutants.**

263 To determine whether the skeletal phenotypes seen in the germline heterozygous
264 mutant mice were caused by defects in the osteoblast lineage, we crossed all our
265 mutant models (*Recql4*$^{K525A/+}$, *Recql4*$^{R347X/+}$ and *Recql4*$^{G522Efs/+}$) to the *Osx*-Cre
266 *Recql4*$^{fl/fl}$ mice (22, 30). This allowed us to delete the wild-type *Recql4* allele from the
267 osteoblastic lineage, leaving only the mutant protein expressed. These osteoblast-
268 restricted point mutant models were compared to *Osx*-Cre+ *Recql4*$^{fl/+}$ mice to control
269 for the known effects of the *Osx*-Cre transgene on bone homeostasis (31, 32)
270 allowing comparison across all Cre+ models. Furthermore, this approach also

bypassed the lethality of homozygous mutant mice and the assessment of cells only expressing truncated proteins in adult mice.

The analysis showed that only the *Osx*-Cre *Recql4*$^{\Delta/R347X}$ mice had a lower body weight and tibial length compared with *Osx*-Cre *Recql4*$^{\Delta/+}$ littermates (Fig 3A and 3B). The *Osx*-Cre *Recql4*$^{\Delta/G522Efs}$ mice had a reduction in body weight, but it did not reach statistical significance (p=0.09) (Fig 3A). Additionally, trabecular analysis showed lower trabecular bone volumes by 13% for *Osx*-Cre *Recql4*$^{\Delta/G522Efs}$ and 25% for *Osx*-Cre *Recql4*$^{\Delta/R347X}$ (Fig 3C). Correspondingly, there was a 12% and 23% reduction in trabecular number, respectively, compared to controls (Fig 3D). Trabecular separation was 17% greater in the *Osx*-Cre *Recql4*$^{\Delta/R347}$ mice only (Fig 3E). For cortical bone parameters, only mice carrying the R347X mutation showed an 8% lower periosteal perimeter and 25% lower mean polar moment of inertia consistent with an 8% reduction in mediolateral width and no change in anteroposterior width when compared to controls (Fig 3G-3K). Again, the K525A helicase-inactive mice did not show any detectable phenotypes when compared to controls. All morphological changes are illustrated in the 3D reconstructed images (Fig 3F and 3L). Additional micro-CT parameters are provided in S4 Fig D-F. In summary, these data demonstrate that truncating mutations of RECQL4 disrupt bone microstructure through defects intrinsic to the osteoblast lineage with the more severe phenotype seen in mice expressing the shortest truncated protein (R347X).

Compound heterozygous *Recql4* mutants tolerate ionizing radiation and do not develop osteosarcoma.

Based on previous studies that show that RTS patients have compound heterozygous mutations with one allele more severely truncated than the other (4, 5), we generated compound heterozygous mouse lines combining the G522Efs or R347X mutations with the K525A. Although this approach does not fully mimic RTS,

it allowed us to determine the *in vivo* effects of a truncated allele and a helicase-inactive allele. Surprisingly, the compound heterozygous *Recql4*$^{G522Efs/K525A}$ and *Recql4*$^{R347X/K525A}$ mice were viable, and pups were born at the expected Mendelian ratio (Fig 4A). Moreover, monitoring of aged cohorts demonstrated that *Recql4*$^{G522Efs/K525A}$ and *Recql4*$^{R347X/K525A}$ mice had a normal lifespan compared to WT mice without increased tumor incidence (Fig 4B). All genotypes developed a small number of spontaneous tumors affecting the liver, spleen, thymus, and intestine, however no osteosarcoma was detected in compound heterozygous mice (S1 Table).

Previous studies have reported increased sensitivity of RECQL4 mutant cell lines to ionizing radiation (33, 34). To assess the *in vivo* response of compound heterozygous mutant mice and whether this increased susceptibility to cancer formation, we treated a small cohort of mice with whole-body ionizing radiation. A single sub-lethal dose of 5Gy γ-irradiation was administered to 9-week old *Recql4*$^{G522Efs/K525A}$, *Recql4*$^{R347X/K525A}$ and *Recql4*$^{K525A/+}$ mice as controls. We monitored the cohorts for one year, assessing peripheral blood parameters at several time points to evaluate hematologic recovery (Fig 5C). The efficacy of the radiation was demonstrated by a similar transient reduction in blood cell populations across all genotypes (Fig 4D-4I). After twelve months, all mice were euthanized and autopsies performed. We found that ionizing radiation did not result in abnormal/delayed hematopoietic recovery or failure nor did it result in tumor development with only one intestinal tumor found in a *Recql4*$^{G522Efs/K525A}$ mouse (Fig 4J). Collectively, these results demonstrate that a full-length, even helicase inactive RECQL4, is sufficient to rescue the lethality caused by truncating mutations. They further demonstrate that these compound heterozygous *Recql4* mutations are not sufficient to sensitize murine models to ionizing radiation or to accelerate cancer initiation.

Truncating human RECQL4 mutations fail to rescue *Recql4* deletion, while mutations that conserve the protein are better tolerated.

To analyze the effects of different human RECQL4 mutations and how they compare to our murine models, we utilized the Hoxb8 immortalized myeloid progenitor cells. This is a relevant cell type, given the requirement of RECQL4 for maintenance of this cell population *in vivo* (35). First, we used this system to determine the effects of truncating murine *Recql4* mutations *in vitro*. Hoxb8 immortalized myeloid progenitor cell lines from *R26*-CreER^{T2} *Recql4*$^{fl/+}$, *R26*-CreER^{T2} *Recql4*$^{fl/K525A}$, *R26*-CreER^{T2} *Recql4*$^{fl/R347X}$, and *R26*-CreER^{T2} *Recql4*$^{fl/G522Efs}$ mice were treated with 400nM/mL of 4-hydroxy-tamoxifen to induce Cre recombinase activity and deletion of the floxed wild type *Recql4* allele, leaving only the mutant allele expressed. We achieved successful deletion by day four, as confirmed by PCR for genomic recombination (S5 Fig). The presence of a single *Recql4* wild type allele (fl/+ cells treated with 4-hydroxy-tamoxifen to become Δ/+) did not interfere with the proliferation rates (Fig 5A), nor did the expression of a single helicase-inactive K525A allele (Fig 5B). However, when the floxed allele was deleted in the cells carrying the truncating mutations G522Efs and R347X, a marked decrease of cell proliferation was observed, consistent with the previously described *in vivo* phenotype (15) and demonstrating an essential requirement of the helicase and C-terminal domains deleted in these mutations (Fig 5C and 5D).

Next, we used this cell line model to determine the capacity of different human *RECQL4* mutations to rescue HoxB8 *R26*-CreER *Recql4*$^{\Delta/\Delta}$ myeloid cells, where both alleles of the endogenous murine *Recql4* were deleted. As expected, control fl/fl cells started dying at day four post-tamoxifen as they became *Recql4* null (Fig 5E and S6 Fig). Interestingly, when we expressed the wild type human RECQL4 protein, cell proliferation was not wholly restored, suggesting that overexpression of wild-type RECQL4 can be detrimental (Fig 5F). We further tested the ability of

352 frequent human RTS associated *RECQL4* mutations, including the human
353 equivalents to our murine germline mutations, to rescue Δ/Δ cell proliferation and
354 viability. To do this, we used the same EGFP-fused human RECQL4 mutations:
355 K508A, C525Afs, and R350Gfs (Fig 5G and 5H), described previously and
356 engineered the p.Arg807ProfsTer38 (R807Pfs), p.Gln757* (Q757X) and
357 p.Leu638Pro (L638P) mutations based on recurrent mutations described in RTS
358 patients (4). The analysis showed that the helicase-inactive K508A mutant
359 successfully rescued the Δ/Δ cells (Fig 5G), while both the C525Afs and R350Gfs
360 human mutants did not (Fig 5H and 5I), similar to endogenous murine G522Efs and
361 R347X (Fig 5C and 5D). Both R807Pfs and Q757X mutations rescued the *Recql4*
362 deletion (Fig 5J and 5K), whereas the L638P achieved only partial rescue (Fig 5L).

363 Finally, we visualized the EGFP-RECQL4 localization in HoxB8 *R26*-CreER
364 *Recql4*$^{fl/fl}$. Similar to what we saw in Kusa4b10 cells (Fig 1G), the wild type human
365 RECQL4, the K508A and the R350Gfs proteins were localized in the nucleus, while
366 the C525Afs was poorly expressed (Fig 5M). On the other hand, the R807Pfs and
367 Q757Pfs mutants displayed both nuclear and cytoplasmic localization, while the
368 L638P mutant was located primarily in the cytoplasm. The sizes and expression
369 levels of the predicted protein products were confirmed by Western blotting (S7 Fig).
370 Collectively, these data demonstrate that not all mutations of RECQL4 are
371 functionally equivalent. Mutations that result in severely truncated protein products,
372 due to early stop codons or frameshifts, are more likely to affect transcript stability
373 and localization and are detrimental to both cellular and organismal health. In
374 contrast, mutations that conserve most of the protein are largely tolerable.

375 **Discussion**

376 Since Kitao *et al.* first cloned the *RECQL4* gene more than twenty years ago (36),
377 some inroads have been made in the understanding of these mutations and their
378 contribution to RTS. It is now known that the majority of mutations reported in RTS
379 patients are compound heterozygous mutations, containing at least one truncated
380 allele and mainly impacting the helicase domain (4, 5). This mutational spectrum
381 implied that defects in the helicase region might be the main reason for the
382 phenotypes of RTS. However, we recently showed that mice with a homozygous
383 knock-in mutation that specifically inactivates RECQL4 ATP-dependent helicase
384 activity were strikingly normal in terms of embryonic development, hematopoiesis,
385 and DNA damage repair (15). In the same study, by using a conditional deletion
386 model that allowed the assessment of the effects of mutations after deleting the wild
387 type *Recql4* allele, we found that mice carrying truncating, but not helicase-inactive,
388 mutations developed bone marrow failure (15). This confirmed the deleterious effects
389 of truncating mutations, which led us to investigate the impact of these mutations in
390 other systems.

391 Assessing the reported *RECQL4* mutations (1, 4, 5), RTS patients presenting
392 with two severe truncating mutations are extremely rare. Here, we generated two
393 *Recql4* mutant models with truncating mutations that closely map to those reported in
394 RTS patients, affecting the helicase and C-terminal domain. We did not recover
395 viable homozygous germline mutant pups from either allele. These results are
396 consistent with the human data and suggest that having two severely truncating
397 mutations of *RECQL4* is not tolerated and that there is an essential developmental
398 role for the deleted domains. Furthermore, in addition to lacking essential domains,
399 there is the potential for these mutations to yield aberrantly expressed and localized
400 protein, further contributing to the phenotypes we observed. When we assessed
401 protein levels of the truncating mutants, we were not able to detect the predicted
402 truncating protein product from the G522Efs mutation. This could be either the

consequence of nonsense-mediated mRNA decay or proteasomal degradation. The C525Afs human mutation, which maps closely to the murine G522Efs mutation, showed similar results. On the other hand, the R347X mutation produced a short but stable protein that localized to the nucleus, albeit with reduced relative nucleolar intensity compared to WT or K525A protein. The R350Gfs human mutation (mapping closely to the R347X) had qualitatively similar expression and localization. We assessed the nucleolar localization signals/sequences in the murine and human RECQL4 using NoD program (Nucleolar localization sequence detector; University of Dundee). The analysis indicated that while murine RECQL4 has two putative signals between 253-278aa and 359-386aa, human RECQL4 has two predicted signals at 10-33aa and 370-390aa, consistent with previous analysis (37). Results also showed that the score for the murine sequences is higher than for the human protein. Given that the R347X mutant truncates the protein prior to the second signal (conserved with the human protein) and that we fail to see accumulation from this protein in the nucleolus, it is suggested that this is the primary functional nucleolar localization sequence. However, we cannot exclude that differences in the tags (EGFP for human compared to mCherry for the murine proteins) or the cell lines used impacted the qualitative assessment of localization (38). Taken together, we have shown that *Recql4* truncating mutations affect protein stability and subcellular localization differently and that this phenotype is reproduced using comparable human mutations.

The skeletal system is severely impacted in the majority of RTS patients. A study of 28 RTS subjects examined by radiologic survey found that up to 75% had some form of skeletal abnormality, including abnormal metaphyseal trabeculation, brachymesophalangy, thumb or radial agenesis or hypoplasia (3). Several additional studies have associated loss of RECQL4 with a more systemic skeletal involvement with a high proportion of patients reporting low bone density (3, 39-42). However, to our knowledge, no studies have mapped skeletal defects to specific RECQL4

mutations. We found that heterozygous expression of the truncating alleles was sufficient to cause low trabecular bone mass, impaired growth of cortical bone, and narrower bones, compared to WT controls. Furthermore, we found that truncating mutations affect normal skeletal formation by causing defects in the osteoblast lineage. These findings were comparable to findings we previously reported in an osteoblast lineage restricted knock-out, which showed that complete deletion of *Recql4* in the osteoblast lineage led to reduced bone volume and defects in osteoblast proliferation and maturation (22). This suggested that at least for bone development, having a truncated RECQL4 protein is equivalent to having no RECQL4 at all, which highlights the critical function of the deleted domains in bone homeostasis. Interestingly, an osteochondral-lineage-specific mouse model reported more severe findings than ours. Cao *et al.* used *Prx1*-Cre to delete *Recql4* in early mesenchymal progenitor cells of the limb buds and described a 50% reduction in bone volume and cortical bone area (41). While RECQL4 is clearly needed in the earlier skeletal cell populations, it is important to consider that our models use truncating heterozygous mutations, instead of null alleles. Thereby, any remaining RECQL4 protein in the pre-osteoblast population of our mutants might be sufficient for partial function at this stage and explain the phenotypic differences between models. Lastly, we observed that the R347X mutation, which produced a stable yet shortest predicted protein, led to a more severe bone phenotype than the poorly expressed G522Efs mutation. This suggested that the severity of the defects was proportional to the severity of the truncation, irrespective of protein expression. Furthermore, the fact that the largest truncation caused the most severe bone phenotype suggests that RECQL4 gene dosage is a critical regulator of bone mass, something relatively unknown until now. Collectively, these results demonstrate that heterozygous truncating mutations of RECQL4 cause a haploinsufficient low bone mass phenotype through defects in the osteoblast lineage. Although RTS patients generally present with compound heterozygous mutations, these results highlight the

importance of having a full-length protein for bone development. Furthermore, they raise concerns regarding the osteoporosis status of the parents of RTS patients, which warrants further investigation.

A characteristic feature of syndromes associated with mutations in RECQL4 is cancer predisposition, particularly osteosarcoma, cutaneous epithelial tumors, and hematological malignancies (2, 43, 44). A recent study analyzed pediatric patients with cancer and identified a significant enrichment in heterozygous *RECQL4* loss-of-function variants in those who presented with osteosarcoma (45). This raised the question whether the presence of compound heterozygous *Recql4* mutations in mice is sufficient to initiate tumorigenesis. We found no differences in tumor burden or spectrum in our compound heterozygous mutants compared to wild type controls, even after exposure to γ-irradiation. Furthermore, although previous studies have reported ionizing radiation as a risk factor for the development of sarcomas (46, 47), and truncated RECQL4 products have been associated with hypersensitivity to this agent (48), we did not observe either hematopoietic failure nor osteosarcoma development in our irradiated cohort. It is possible that the non-truncating but helicase-inactive allele is sufficient to rescue these phenotypes and that truncating mutations in both alleles are necessary for tumor initiation. However, this could not be addressed in this study given the developmental lethality seen in our homozygous truncating mice. Another possibility is that larger numbers of mice and longer timepoints are necessary for this phenotype to develop. It is also possible that additional genes are involved in the development of these RTS phenotypes. All these limitations should be addressed in future studies.

Lastly, we established a tractable *in vitro* cell line model, which allowed us to examine the cellular consequences of different *RECQL4* mutations. We found that cells carrying the murine truncating G522Efs and R347X mutations developed a proliferation defect after deletion of the floxed wild-type *Recql4* allele. Similarly, the closely related human C525Afs and R350Gfs mutations failed to rescue the lethality

487 caused by *Recql4 deletion*. On the other hand, the murine ATP-dependent helicase
488 inactive mutation (K525A) did not demonstrate a proliferation defect, and its human
489 counterpart (K508A) successfully rescued *Recql4* deletion. These results confirm
490 that truncating, but not helicase-inactive mutations are pathogenic and that our
491 murine mutations are useful surrogates for understanding the functions of human
492 disease-associated *RECQL4* mutations. When using this system to analyze other
493 human mutations, we found that cells overexpressing the human wild type protein
494 could not completely rescue *Recql4* deletion, suggesting that overexpression of
495 RECQL4 is not well tolerated. In fact, several studies have correlated overexpression
496 of *RECQL4* with the development of malignancies (49-54). We also found that the
497 L638P mutation, which resulted in a stable full-length product with cytoplasmic
498 localization, could not fully rescue the *Recql4* deletion. This demonstrates that in
499 order for RECQL4 to function effectively, it needs to be located within the nucleus.
500 Finally, the R807Pfs and Q757X mutations, which have been found in RTS patients
501 with osteosarcoma and lymphomas (4), were able to rescue the *Recql4* deletion.
502 This indicates that small C-terminal deletions do not severely affect viability, unlike
503 larger deletions that include both the helicase and the C-terminal domains. However,
504 their association with malignancies remains unknown. By comparing different
505 mutations in the same genetic context, this system allowed us to conclude that the
506 different mutations have distinct consequences for RECQL4. While some mutations
507 create unstable proteins, some alter its localization without grossly affecting protein
508 stability. Overall, the level of the truncation appeared to show the strongest
509 correlation with the severity of the phenotype. Given the increasing number of
510 somatic *RECQL4* mutations reported in sporadic cancers, this *in vitro* system can
511 serve as a platform to assess the impact of *RECQL4* mutations at a cellular level.

512 In conclusion, truncating RECQL4 mutations affect protein stability and
513 localization, contributing to the development of an osteoporosis-like phenotype
514 through defects in early osteoblast progenitors in mice. However, they are not

515 sufficient to promote tumorigenesis, even after exposure to irradiation. Future studies
516 should focus on the identification of genes that co-operate with RECQL4 in normal
517 development and tumorigeneses. These will allow a better understanding of the
518 genetic landscape of RTS and permit the generation of more comprehensive models.
519

Materials and Methods

Ethics Statement

All animal experiments conducted for this study were approved by the Animal Ethics Committee of St. Vincent's Hospital, Melbourne, Australia (#007/14, 011/15, and 015/17). Animals were euthanized by cervical dislocation or CO_2 asphyxiation.

Mice

The chemically (ENU, N-ethyl-N-nitrosourea) induced *Recql4*^{R347X} point mutation was provided by the Australian Phenomics Facility (APF, Canberra, Australia; allele IGL01809). *Recql4*^{G522Efs} mice were identified during CRISPR/Cas9 targeting to generate the previously described *Recql4*^{K525A} mutation (15) by the Mouse Engineering at Garvan/ABR (MEGA) service (Garvan Institute, Darlinghurst, Australia). This allele is on a C57BL/6 background and carried a 2bp insertion (GA) after the T521 codon. The *Osx*-Cre, *Rosa26*-eYFP, and *Recql4*^{K525A} mutant animals have been previously described (15, 22, 30). *Rosa26*-CreER^{T2} mice were originally purchased from The Jackson Laboratory (B6.129-*Gt(ROSA)26Sor*$^{tm1(cre/ERT2)Tyj}$/J, Stock Number: 008463) and have been previously described (35). The ENU derived mutant (*Recql4*^{R347X}) was backcrossed to C57BL/6 at least six times and evaluated across multiple generations. All lines were on a C57BL/6 background. All animals were housed at the BioResources Centre (BRC) at St. Vincent's Hospital. Mice were maintained and bred under specific pathogen-free conditions with food and water provided *ad libitum.*

All mouse lines are available from the Australian Phenome Bank (APB; https://pb.apf.edu.au/). Strain identification numbers/names are: R347X (APB ID#7986); *R26*-CreER *Recql4*$^{fl/fl}$ (APB ID#7263); *Osx*-Cre *R26*-eYFP *Recql4*$^{fl/fl}$ (APB ID#7886); K525A (strain name: C57BL/6-Recql4<tm4Crw>) and G522Efs (strain name: C57BL/6-Recql4<tm5Crw>).

Cloning of mCherry and EGFP RECQL4 proteins and Retroviral production

Human N terminal EGFP fused RECQL4 and EGFP fused RECQL4^{K508A} (provided by T. Enomoto, Musashino University, Tokyo, Japan; (55)) were cloned into MSCV-puro (35). Human mutations R807Pfs, Q757X, L638P, C525Afs, and R350Gfs, were created by gBlock (IDT) replacement of a wild-type fragment of EGFP-RECQL4 in the plasmid MSCV-puro with a mutant fragment. Murine mCherry fused RECQL4 was assembled from a codon-optimized synthetic m*Recql4* cDNA (GeneArt, Life Technologies), placed in frame with an N-terminal mCherry cDNA (gBlock, IDT) in MSCV-puro. Mouse mutations were created by gBlock (IDT) replacement of the required fragment of *Recql4*. All constructs contain full-length cDNAs, including those coding for truncating mutations. All mutations were confirmed by Sanger sequencing. Retrovirus was produced by transient transfection of 293T cells using calcium phosphate mediated transfection with an ecotropic packaging plasmid (35).

Genotyping

Genotyping of the G522Efs mutants was determined by PCR using the following primers: mRecql4 K525A MO36-R3: 5'-AGAACATTGGGCATTCGGC-3' and mRecql4 K525A MO36-F9: 5'-TAGACCTTATGAAACCTCAAAGCC-3' to obtain a 591bp product, which was then digested with *MslI* (NEB) to generate three fragments of 347, 175 and 71bp for the G522Efs mutant; or two fragments of 416 and 175bp for the WT. Genotyping of the K525A mutants has been previously described and used the same primers and restriction enzyme as the G522Efs mutation with the difference that this resulted in three fragments of 361, 175, and 55bp (15). The presence of the R347X mutation was determined by KASP (competitive allele-specific PCR) technology (LGC) with facility provided primers: 5'-GAAGGTGACCAAGTTCATGCTAAAGCGTTTGTTTTTCATGTTGAGTCG-3', 5'-GAAGGTCGGAGTCAACGGATTCAAAGCGTTTGTTTTTCATGTTGAGTCA-3', and

reverse primer 5'-GCTTCCCTAGACAGAGGGAACTATA-3' used according to manufacturer instructions.

Protein extraction and Western blotting

Thymocyte lysates from germline *Recql4*$^{R347X/+}$ and *Recql4*$^{G522Efs/+}$ were prepared in RIPA buffer (50mM Tris, 150mM NaCl, 1% NP-40, 0.5% sodium deoxycholate, 0.1% SDS, pH8.0) plus Complete protease inhibitor (Roche) and PhosStop (Roche) tablets. Protein was quantified using the Pierce BCA protein assay kit (Thermo Fisher Scientific) on an Enspire multimode plate reader (Perkin Elmer). Lysates from HoxB8 immortalized (25) *R26*-CreER^{T2} *Recql4*$^{fl/G522Efs}$, *R26*-CreER^{T2} *Recql4*$^{fl/R347X}$ and *R26*-CreER^{T2} *Recql4*$^{+/+}$ transduced with MSCV puro 3xFlag-RECQL4 were prepared in sample buffer (2x10^6 cells in 100μl). 50μg of whole protein extracts from thymocytes and 50μl from myeloid cells were loaded on pre-cast NuPAGE™ BOLT 8% Bis-Tris polyacrylamide gels (Invitrogen) and transferred onto Immobilon-P PVDF membranes (Merck Millipore). Membranes were blocked with 5% milk in Tris-buffered saline with tween (TBST) and incubated at 4°C overnight with rat monoclonal anti-mouse RECQL4 antibody (clone 3B10, detects mouse; or clone 3B1, detects both human and mouse) (15), mouse anti-Actin (Sigma Aldrich, A1978), or anti-Flag antibody (Sigma Aldrich). Membranes were then probed with HRP-conjugated goat anti-rat (Thermo Fisher Scientific, 31470) or anti-mouse (Thermo Fisher Scientific, 31444) secondary antibodies and visualized using ECL Prime Reagent for chemiluminescent detection on Hyperfilm ECL (Amersham). The predicted molecular weight for the truncated proteins is 62.4kDa for G522Efs, 65.6kDa for 3xFlag-G522Efs, 38.1kDa for R347X, and 41.3kDa for 3xFlag-R347X.

Live cell imaging and image processing of RECQL4 fusion proteins

602 Transduced osteoblast-like Kusa4b10 cells were plated in 10-cm dishes, selected
603 with puromycin, and grown to sub-confluency. Single plane images were acquired on
604 an inverted fluorescent microscope (Olympus IX81) with a 40X objective (LUCPLFLN
605 40X) and were recorded with a Retiga-EXi 12 Bit CCD camera (QImaging). Image
606 processing and analysis were done using MetaMorph (Molecular Devices) and
607 Adobe Photoshop. HoxB8 immortalized myeloid cells were concentrated by
608 centrifugation and 5µl of cell suspension dispensed on a slide before image
609 acquisition with a 60X objective (UPLANAPO 60X water immersion). For
610 mitochondrial staining, 250µL of Mitochondrial Staining Solution (CytoPainter
611 MitoBlue Indicator Reagent (ab219940), 1:500 diluted in Hank's Balanced Salt
612 solution + 20 mM HEPES buffer (HHBS)) was added to Kusa4b10 cells grown on
613 coverslips in 250µL DMEM in a 24-well plate and incubated for 30 minutes to 2 hours
614 in a 37ºC/5% CO_2 incubator. Coverslips were washed twice with HHBS, and live cells
615 were imaged as described above.
616
617 **Seahorse XF24 Extracellular Flux analyzer**
618 Hoxb8 immortalized (25) *R26*-CreER^{T2} *Recql*$^{fl/+}$ (control), *R26*-CreER^{T2} *Recql4*$^{fl/K525A}$,
619 *R26*-CreER^{T2} *Recql4*$^{fl/G522Efs}$, and *R26*-CreER^{T2} *Recql4*$^{fl/R347X}$ myeloid cells were
620 maintained in IMDM, 10% FBS (non-heat inactivated) and 1% GM-CSF containing
621 media (BHK-HM5 cell-conditioned media). The cells were treated for four days with
622 400nM 4-hydroxy tamoxifen (Merck Millipore) then genotyped to confirm complete
623 recombination. To adhere myeloid (suspension) cells to the XF24 cell culture plate,
624 wells were first coated with 100µl of RetroNectin solution (32µg/ml in PBS, Takara
625 Bio), incubated for 2 hours at room temperature, then blocked with 200µl of 2% BSA
626 in PBS, and washed with PBS. Cells were then seeded at 120,000 cells/well and
627 spun at 1100g for 20 seconds. Cell culture media was replaced with non-buffered
628 DMEM base media (Seahorse bioscience) containing 25mM glucose, 1mM sodium

pyruvate, glutamine at pH 7.4, and incubated for 1 hour at 37°C in a non-CO_2 incubator. The oxygen consumption rate (OCR) was measured in a Seahorse XF24-3 Flux Analyzer. Cells were assayed with a 2-min mix/2-min wait/5-min measurement cycle for three baseline measurements followed by three cycles after each injection of four compounds affecting bioenergetics: 0.5μM oligomycin (Complex V inhibitor; Sigma, St. Louis, MO, USA), 0.7μM carbonyl cyanide 4-(trifluoromethoxy)phenylhydrazone (FCCP; $\Delta\Psi_m$ uncoupler; Sigma), 3.6μM antimycin A (Complex III inhibitor; Sigma), and 6μM rotenone (Complex I inhibitor; Sigma). After completion of the analysis, Cyquant (Life technologies) was used to normalize measurements to cell number in the corresponding wells.

Micro-Computed tomography (micro-CT) 3D analysis of tibia

Tibiae were collected from mutant mice and their littermate controls; the attached soft tissue was removed carefully, and tibiae were fixed in 2% paraformaldehyde overnight, which was then replaced by 70% ethanol. Tibia morphology and microarchitecture was analyzed by ex-vivo micro-CT on the left tibia wrapped in 70% ethanol-soaked gauze within a cryovial by using a Skyscan 1076 system (Bruker MicroCT, Kontich, Belgium). Images were acquired at 9μm pixel size, 0.5mm aluminum filter, 44kV voltage, 220μA current, 2300ms exposure time, 0.5° rotation, 1 frame averaging. Image slices were reconstructed by NRecon (Bruker, version 1.6.10.2) using the following settings: 36% beam-hardening correction, 6 ring artifact correction, 1 smoothing, and no defect pixel masking. The reconstructed images were analyzed with software programs Dataviewer (Bruker, version 1.4.4), CTan (Bruker, version 1.15.4.0), and CTVox (Bruker, version 2.4.0). The trabecular and cortical region of interest (ROI) was determined by identifying the start of the mineralized zone of the proximal growth plate and calculating a distance equal to 3.5% and 40% of the total tibial length, respectively. From that point, a further 5% of

the total tibial length was analyzed as the secondary spongiosa trabecular ROI and a 5% as the cortical ROI. Analysis of bone structure was completed by adaptative thresholding in CTan, which was determined by performing automatic thresholding on 3 samples from each experimental group resulting in threshold values of 50-255 for trabecular bone and 90-255 for cortical bone. Representative images of reconstructed trabecular and cortical bone with color-coded quantitative mineralization were made of the specimen whose value was closest to the group mean using the trabecular bone volume and cortical thickness parameters.

Peripheral blood analysis

Peripheral blood (approximately 100μl) was obtained via retro-orbital bleeding. 25μl of blood was mixed with 75μl of PBS to obtain cell counts on a hematological analyzer (Sysmex KX-21N, Roche Diagnostics). The remaining blood was red blood cell-depleted using hypotonic lysis buffer (150mM NH_4Cl, 10mM $KHCO_3$, 0.1mM Na_2EDTA, pH7.3) and resuspended in 150μl of FACS buffer for flow cytometry analysis.

Flow cytometry analysis

Bones were flushed, spleens and thymus crushed, and single-cell suspensions were prepared in FACS buffer. Antibodies against murine Ter119, CD71, B220, IgM, CD43, CD19, CD21, CD23, Mac-1, Gr1, F4/80, CD4, CD8, TCRβ, CD25, CD44, Sca-1, c-Kit, CD34, FLT3, FcγRII/III (CD16/32), CD41, CD105, CD150, either biotinylated or conjugated with phycoerythrin, phycoerythrin-Cy7, peridinin chlorophyll protein-Cy5.5, allophycocyanin, allophycocyanin eFluor780, eFluor660 or eFluor450 were all obtained from eBioscience, BioLegend or BD Pharmingen (S2 Table) (15, 35, 56, 57). Biotinylated antibodies were detected with streptavidin-conjugated with Brilliant

682 Violet-605. 30,000-500,000 cells were acquired on a BD LSRIIFortessa and analyzed
683 with FlowJo software Version 9 or 10.0 (Treestar).
684
685 **Cell proliferation assays**
686 Hoxb8 immortalized (25) *R26*-CreER^{T2} *Recq4l*$^{fl/+}$, *R26*-CreER^{T2} *Recql4*$^{fl/G522Efs}$, and
687 *R26*-CreER^{T2} *Recql4*$^{fl/R347X}$ cells were maintained in IMDM, 10% FBS (non-heat
688 inactivated), 1% Pen/Strep, 1% L-Glutamine, and 1% GM-CSF containing media
689 (BHK-HM5 cell-conditioned media). The cells were treated for 14 days with 400nM 4-
690 hydroxy tamoxifen (Merck Millipore) then genotyped to confirm complete
691 recombination. Cells were counted with Trypan blue using a Countess II automated
692 counter (Thermo Fisher Scientific) and then split every two-three days.
693
694 **Retroviral transduction and complementation**
695 Hoxb8 immortalized *R26*-CreER^{T2} *Recql4*$^{fl/fl}$ cells were maintained in IMDM, 10%
696 FBS (non-heat inactivated), 1% Pen/Strep, 1% L-Glutamine, and 1% GM-CSF
697 containing media (BHK-HM5 cell-conditioned media). Exponentially growing Hoxb8
698 *R26*-CreER^{T2} *Recql4*$^{fl/fl}$ cells (100,000 cells/mL) were spin-infected with EGFP-
699 RECQL4 retrovirus in a 1:1 ratio at 1100g for 90 minutes in 8µg/mL polybrene. Two
700 days after infection, cells were selected with puromycin (0.25µg/mL) for four days
701 and then expanded. Cells were then treated for 14 days with 400nM 4-hydroxy
702 tamoxifen (Merck Millipore) and genotyped to confirm complete recombination. Cells
703 were counted with Trypan blue using a Countess II automated counter (Thermo
704 Fisher Scientific) and then split every two-three days.
705
706 **Statistical analysis**
707 To determine statistical significance, Kaplan-Meier survival plots and ordinary one-
708 way ANOVA tests were conducted in Prism software version 8 (GraphPad; San
709 Diego, CA, USA). Throughout this study, significance is indicated using the following

710 convention: *P<0.05; **P<0.01; ***P<0.001; ****P<0.0001, and data is presented as
711 mean ± S.E.M. Furthermore, the number of samples used for each experiment is
712 described in the corresponding figure legends
713

Acknowledgments

We thank R. Brink and the Mouse Engineering Garvan/ABR (MEGA) Facility (Garvan Institute, Sydney, Australia) for the generation of the G522Efs allele; the Australian Phenomics Facility and the Australian National University (Canberra, Australia) for their technical expertise and provision of the R347X allele; S Galic and L Murray-Segal (St Vincent's Institute) for training on Echo-MRI; T. Enomoto (Musashino University, Tokyo, Japan) for providing human EGFP-RECQL4 WT and K508A constructs; M. Kamps (University of California San Diego, USA) for providing the Hoxb8 vectors used to generate cell lines; D. Thorburn (Murdoch Children's Research Institute and University of Melbourne, Australia) and J. Heierhorst (St Vincent's Institute) for comments on the manuscript.

Author contribution statement:

Conceptualization: Wilson Castillo-Tandazo, Monique F. Smeets, Carl R. Walkley.

Funding acquisition: Carl R. Walkley.

Investigation: Wilson Castillo-Tandazo, Ann E. Frazier, Monique F. Smeets, Carl R. Walkley.

Methodology: Wilson Castillo-Tandazo, Ann E. Frazier, Natalie A Sims, Monique F. Smeets, Carl R. Walkley.

Project administration: Monique F. Smeets, Carl R. Walkley.

Supervision: Monique F. Smeets, Carl R. Walkley.

Visualization: Wilson Castillo-Tandazo, Monique F. Smeets, Carl R. Walkley.

Writing – original draft: Wilson Castillo-Tandazo, Monique F. Smeets, Carl R. Walkley.

Writing – review & editing: Wilson Castillo-Tandazo, Ann E. Frazier, Natalie A. Sims, Monique F. Smeets, Carl R. Walkley.

Funding

This work was supported by the Office of the Assistant Secretary of Defense for Health Affairs through the Peer Reviewed Cancer Research under Award No. W81XWH-15-1-0315 (to C.R.W.). Opinions, interpretations, conclusions, and recommendations are those of the author and are not necessarily endorsed by the Department of Defense (USA); National Health and Medical Research Council (NHMRC) Australia project grant (to C.R.W., APP1102004); a Melbourne Research Scholarship (to W.C-T. University of Melbourne); Victorian Cancer Agency Research Fellowship (to C.R.W. MCRF15015); Mito Foundation (to A.E.F.). This work was enabled by the Australian Phenomics Network and partly supported by funding from the Australian Government's National Collaborative Research Infrastructure Strategy and the Super Science Initiative through the Education Investment Fund (to Australian Phenomics Network); and in part by the Victorian State Government Operational Infrastructure Support (to St Vincent's Institute and Murdoch Children's Research Institute).

The funders had no role in study design, data collection, and analysis, decision to publish, or preparation of the manuscript.

References

1. Larizza L, Roversi G, Volpi L. 2010. Rothmund-Thomson syndrome. Orphanet J Rare Dis 5:2.
2. Wang LL, Levy ML, Lewis RA, Chintagumpala MM, Lev D, Rogers M, Plon SE. 2001. Clinical manifestations in a cohort of 41 Rothmund-Thomson syndrome patients. Am J Med Genet 102:11-7.
3. Mehollin-Ray AR, Kozinetz CA, Schlesinger AE, Guillerman RP, Wang LL. 2008. Radiographic abnormalities in Rothmund-Thomson syndrome and genotype-phenotype correlation with RECQL4 mutation status. AJR Am J Roentgenol 191:W62-6.
4. Siitonen HA, Sotkasiira J, Biervliet M, Benmansour A, Capri Y, Cormier-Daire V, Crandall B, Hannula-Jouppi K, Hennekam R, Herzog D, Keymolen K, Lipsanen-Nyman M, Miny P, Plon SE, Riedl S, Sarkar A, Vargas FR, Verloes A, Wang LL, Kaariainen H, Kestila M. 2009. The mutation spectrum in RECQL4 diseases. Eur J Hum Genet 17:151-8.
5. Wang LL, Gannavarapu A, Kozinetz CA, Levy ML, Lewis RA, Chintagumpala MM, Ruiz-Maldanado R, Contreras-Ruiz J, Cunniff C, Erickson RP, Lev D, Rogers M, Zackai EH, Plon SE. 2003. Association between osteosarcoma and deleterious mutations in the RECQL4 gene in Rothmund-Thomson syndrome. J Natl Cancer Inst 95:669-74.
6. Ajeawung NF, Nguyen TTM, Lu L, Kucharski TJ, Rousseau J, Molidperee S, Atienza J, Gamache I, Jin W, Plon SE, Lee BH, Teodoro JG, Wang LL, Campeau PM. 2019. Mutations in ANAPC1, Encoding a Scaffold Subunit of the Anaphase-Promoting Complex, Cause Rothmund-Thomson Syndrome Type 1. Am J Hum Genet 105:625-30.
7. Kitao S, Shimamoto A, Goto M, Miller RW, Smithson WA, Lindor NM, Furuichi Y. 1999. Mutations in RECQL4 cause a subset of cases of Rothmund-Thomson syndrome. Nat Genet 22:82-4.

8. Wang LL, Worley K, Gannavarapu A, Chintagumpala MM, Levy ML, Plon SE. 2002. Intron-size constraint as a mutational mechanism in Rothmund-Thomson syndrome. Am J Hum Genet 71:165-7.

9. Ohlenschlager O, Kuhnert A, Schneider A, Haumann S, Bellstedt P, Keller H, Saluz HP, Hortschansky P, Hanel F, Grosse F, Gorlach M, Pospiech H. 2012. The N-terminus of the human RecQL4 helicase is a homeodomain-like DNA interaction motif. Nucleic Acids Res 40:8309-24.

10. Gaggioli V, Zeiser E, Rivers D, Bradshaw CR, Ahringer J, Zegerman P. 2014. CDK phosphorylation of SLD-2 is required for replication initiation and germline development in C. elegans. J Cell Biol 204:507-22.

11. Keller H, Kiosze K, Sachsenweger J, Haumann S, Ohlenschlager O, Nuutinen T, Syvaoja JE, Gorlach M, Grosse F, Pospiech H. 2014. The intrinsically disordered amino-terminal region of human RecQL4: multiple DNA-binding domains confer annealing, strand exchange and G4 DNA binding. Nucleic Acids Res 42:12614-27.

12. Shamanna RA, Singh DK, Lu H, Mirey G, Keijzers G, Salles B, Croteau DL, Bohr VA. 2014. RECQ helicase RECQL4 participates in non-homologous end joining and interacts with the Ku complex. Carcinogenesis 35:2415-24.

13. Xu X, Rochette PJ, Feyissa EA, Su TV, Liu Y. 2009. MCM10 mediates RECQ4 association with MCM2-7 helicase complex during DNA replication. EMBO J 28:3005-14.

14. Fairman-Williams ME, Guenther UP, Jankowsky E. 2010. SF1 and SF2 helicases: family matters. Curr Opin Struct Biol 20:313-24.

15. Castillo-Tandazo W, Smeets MF, Murphy V, Liu R, Hodson C, Heierhorst J, Deans AJ, Walkley CR. 2019. ATP-dependent helicase activity is dispensable for the physiological functions of Recql4. PLoS Genet 15:e1008266.

16. Kaiser S, Sauer F, Kisker C. 2017. The structural and functional characterization of human RecQ4 reveals insights into its helicase mechanism. Nat Commun 8:15907.

17. Petkovic M, Dietschy T, Freire R, Jiao R, Stagljar I. 2005. The human Rothmund-Thomson syndrome gene product, RECQL4, localizes to distinct nuclear foci that

coincide with proteins involved in the maintenance of genome stability. J Cell Sci 118:4261-9.

18. Woo LL, Futami K, Shimamoto A, Furuichi Y, Frank KM. 2006. The Rothmund-Thomson gene product RECQL4 localizes to the nucleolus in response to oxidative stress. Exp Cell Res 312:3443-57.

19. Hicks MJ, Roth JR, Kozinetz CA, Wang LL. 2007. Clinicopathologic features of osteosarcoma in patients with Rothmund-Thomson syndrome. J Clin Oncol 25:370-5.

20. Ferrari S, Smeland S, Mercuri M, Bertoni F, Longhi A, Ruggieri P, Alvegard TA, Picci P, Capanna R, Bernini G, Muller C, Tienghi A, Wiebe T, Comandone A, Bohling T, Del Prever AB, Brosjo O, Bacci G, Saeter G, Italian, Scandinavian Sarcoma G. 2005. Neoadjuvant chemotherapy with high-dose Ifosfamide, high-dose methotrexate, cisplatin, and doxorubicin for patients with localized osteosarcoma of the extremity: a joint study by the Italian and Scandinavian Sarcoma Groups. J Clin Oncol 23:8845-52.

21. Lu L, Harutyunyan K, Jin W, Wu J, Yang T, Chen Y, Joeng KS, Bae Y, Tao J, Dawson BC, Jiang MM, Lee B, Wang LL. 2015. RECQL4 Regulates p53 Function In Vivo During Skeletogenesis. J Bone Miner Res 30:1077-89.

22. Ng AJ, Walia MK, Smeets MF, Mutsaers AJ, Sims NA, Purton LE, Walsh NC, Martin TJ, Walkley CR. 2015. The DNA helicase recql4 is required for normal osteoblast expansion and osteosarcoma formation. PLoS Genet 11:e1005160.

23. Chi Z, Nie L, Peng Z, Yang Q, Yang K, Tao J, Mi Y, Fang X, Balajee AS, Zhao Y. 2012. RecQL4 cytoplasmic localization: implications in mitochondrial DNA oxidative damage repair. Int J Biochem Cell Biol 44:1942-51.

24. Croteau DL, Rossi ML, Canugovi C, Tian J, Sykora P, Ramamoorthy M, Wang ZM, Singh DK, Akbari M, Kasiviswanathan R, Copeland WC, Bohr VA. 2012. RECQL4 localizes to mitochondria and preserves mitochondrial DNA integrity. Aging Cell 11:456-66.

25. Wang GG, Calvo KR, Pasillas MP, Sykes DB, Häcker H, Kamps MP. 2006. Quantitative production of macrophages or neutrophils ex vivo using conditional Hoxb8. Nature Methods 3:287-93.

26. Broom MA, Wang LL, Otta SK, Knutsen AP, Siegfried E, Batanian JR, Kelly ME, Shah M. 2006. Successful umbilical cord blood stem cell transplantation in a patient with Rothmund-Thomson syndrome and combined immunodeficiency. Clin Genet 69:337-43.

27. De Somer L, Wouters C, Morren MA, De Vos R, Van Den Oord J, Devriendt K, Meyts I. 2010. Granulomatous skin lesions complicating Varicella infection in a patient with Rothmund-Thomson syndrome and immune deficiency: case report. Orphanet J Rare Dis 5:1-5.

28. Rudilla F, Franco-Jarava C, Martinez-Gallo M, Garcia-Prat M, Martin-Nalda A, Riviere J, Aguilo-Cucurull A, Mongay L, Vidal F, Solanich X, Irastorza I, Santos-Perez JL, Tercedor Sanchez J, Cusco I, Serra C, Baz-Redon N, Fernandez-Cancio M, Carreras C, Vagace JM, Garcia-Patos V, Pujol-Borrell R, Soler-Palacin P, Colobran R. 2019. Expanding the Clinical and Genetic Spectra of Primary Immunodeficiency-Related Disorders With Clinical Exome Sequencing: Expected and Unexpected Findings. Front Immunol 10:2325.

29. Ho MS, Medcalf RL, Livesey SA, Traianedes K. 2015. The dynamics of adult haematopoiesis in the bone and bone marrow environment. Br J Haematol 170:472-86.

30. Rodda SJ, McMahon AP. 2006. Distinct roles for Hedgehog and canonical Wnt signaling in specification, differentiation and maintenance of osteoblast progenitors. Development 133:3231-44.

31. Davey RA, Clarke MV, Sastra S, Skinner JP, Chiang C, Anderson PH, Zajac JD. 2012. Decreased body weight in young Osterix-Cre transgenic mice results in delayed cortical bone expansion and accrual. Transgenic Res 21:885-93.

32. Huang W, Olsen BR. 2015. Skeletal defects in Osterix-Cre transgenic mice. Transgenic Res 24:167-72.

33. Jin W, Liu H, Zhang Y, Otta SK, Plon SE, Wang LL. 2008. Sensitivity of RECQL4-deficient fibroblasts from Rothmund-Thomson syndrome patients to genotoxic agents. Hum Genet 123:643-53.

34. Kohzaki M, Ootsuyama A, Sun L, Moritake T, Okazaki R. 2020. Human RECQL4 represses the RAD52-mediated single-strand annealing pathway after ionizing radiation or cisplatin treatment. Int J Cancer 146:3098-3113.

35. Smeets MF, DeLuca E, Wall M, Quach JM, Chalk AM, Deans AJ, Heierhorst J, Purton LE, Izon DJ, Walkley CR. 2014. The Rothmund-Thomson syndrome helicase RECQL4 is essential for hematopoiesis. J Clin Invest 124:3551-65.

36. Kitao S, Ohsugi I, Ichikawa K, Goto M, Furuichi Y, Shimamoto A. 1998. Cloning of two new human helicase genes of the RecQ family: biological significance of multiple species in higher eukaryotes. Genomics 54:443-52.

37. Burks LM, Yin J, Plon SE. 2007. Nuclear import and retention domains in the amino terminus of RECQL4. Gene 391:26-38.

38. Martin RM, Ter-Avetisyan G, Herce HD, Ludwig AK, Lattig-Tunnemann G, Cardoso MC. 2015. Principles of protein targeting to the nucleolus. Nucleus 6:314-25.

39. Barisonek KL, Protzman NM, Wobst GM, Brigido SA. 2016. Delayed Union of a Jones Fracture in a Patient With Rothmund-Thomson Syndrome: A Case Report and Review of the Literature. J Foot Ankle Surg 55:291-3.

40. Beckmann N. 2015. Multiple Low Energy Long Bone Fractures in the Setting of Rothmund-Thomson Syndrome. Case Rep Med 2015:495164.

41. Cao F, Lu L, Abrams SA, Hawthorne KM, Tam A, Jin W, Dawson B, Shypailo R, Liu H, Lee B, Nagamani SCS, Wang LL. 2017. Generalized metabolic bone disease and fracture risk in Rothmund-Thomson syndrome. Hum Mol Genet 26:3046-55.

42. Carlson AM, Thomas KB, Kirmani S, Lindor NM. 2012. Chronic tibial nonunion in a Rothmund-Thomson syndrome patient. Am J Med Genet A 158A:2250-3.

43. Simon T, Kohlhase J, Wilhelm C, Kochanek M, De Carolis B, Berthold F. 2010. Multiple malignant diseases in a patient with Rothmund-Thomson syndrome with RECQL4 mutations: Case report and literature review. Am J Med Genet A 152A:1575-9.

44. Stinco G, Governatori G, Mattighello P, Patrone P. 2008. Multiple cutaneous neoplasms in a patient with Rothmund-Thomson syndrome: case report and published work review. J Dermatol 35:154-61.

45. Maciaszek JL, Oak N, Chen W, Hamilton KV, McGee RB, Nuccio R, Mostafavi R, Hines-Dowell S, Harrison L, Taylor L, Gerhardt EL, Ouma A, Edmonson MN, Patel A, Nakitandwe J, Pappo AS, Azzato EM, Shurtleff SA, Ellison DW, Downing JR, Hudson MM, Robison LL, Santana V, Newman S, Zhang J, Wang Z, Wu G, Nichols KE, Kesserwan CA. 2019. Enrichment of heterozygous germline RECQL4 loss-of-function variants in pediatric osteosarcoma. Cold Spring Harb Mol Case Stud 5:a004218.

46. Huvos AG, Woodard HQ. 1988. Postradiation sarcomas of bone. Health Phys 55:631-6.

47. Virtanen A, Pukkala E, Auvinen A. 2006. Incidence of bone and soft tissue sarcoma after radiotherapy: a cohort study of 295,712 Finnish cancer patients. Int J Cancer 118:1017-21.

48. Kohzaki M, Chiourea M, Versini G, Adachi N, Takeda S, Gagos S, Halazonetis TD. 2012. The helicase domain and C-terminus of human RecQL4 facilitate replication elongation on DNA templates damaged by ionizing radiation. Carcinogenesis 33:1203-10.

49. Maire G, Yoshimoto M, Chilton-MacNeill S, Thorner PS, Zielenska M, Squire JA. 2009. Recurrent RECQL4 imbalance and increased gene expression levels are associated with structural chromosomal instability in sporadic osteosarcoma. Neoplasia 11:260-8.

50. Saglam O, Shah V, Worsham MJ. 2007. Molecular differentiation of early and late stage laryngeal squamous cell carcinoma: an exploratory analysis. Diagn Mol Pathol 16:218-21.

51. Thomassen M, Tan Q, Kruse TA. 2009. Gene expression meta-analysis identifies chromosomal regions and candidate genes involved in breast cancer metastasis. Breast Cancer Res Treat 113:239-49.

52. Buffart TE, Coffa J, Hermsen MA, Carvalho B, van der Sijp JR, Ylstra B, Pals G, Schouten JP, Meijer GA. 2005. DNA copy number changes at 8q11-24 in metastasized colorectal cancer. Cell Oncol 27:57-65.

53. Narayan G, Bourdon V, Chaganti S, Arias-Pulido H, Nandula SV, Rao PH, Gissmann L, Durst M, Schneider A, Pothuri B, Mansukhani M, Basso K, Chaganti RS, Murty VV.

2007. Gene dosage alterations revealed by cDNA microarray analysis in cervical cancer: identification of candidate amplified and overexpressed genes. Genes Chromosomes Cancer 46:373-84.

54. Chen H, Yuan K, Wang X, Wang H, Wu Q, Wu X, Peng J. 2018. Overexpression of RECQL4 is associated with poor prognosis in patients with gastric cancer. Oncol Lett 16:5419-25.

55. Abe T, Yoshimura A, Hosono Y, Tada S, Seki M, Enomoto T. 2011. The N-terminal region of RECQL4 lacking the helicase domain is both essential and sufficient for the viability of vertebrate cells. Role of the N-terminal region of RECQL4 in cells. Biochim Biophys Acta 1813:473-9.

56. Liddicoat BJ, Piskol R, Chalk AM, Ramaswami G, Higuchi M, Hartner JC, Li JB, Seeburg PH, Walkley CR. 2015. RNA editing by ADAR1 prevents MDA5 sensing of endogenous dsRNA as nonself. Science 349:1115-20.

57. Singbrant S, Russell MR, Jovic T, Liddicoat B, Izon DJ, Purton LE, Sims NA, Martin TJ, Sankaran VG, Walkley CR. 2011. Erythropoietin couples erythropoiesis, B-lymphopoiesis, and bone homeostasis within the bone marrow microenvironment. Blood 117:5631-42.

Figure Legends

Fig. 1. Truncating RECQL4 mutations G522Efs and R347X affect protein expression and localization differently and are homozygous embryo lethal. (A) Schematic illustration of RECQL4 mutations reported in RTS patients and murine mutations used in this study. Image generated using Protein Painter (PeCan portal, St Jude's). (B) *Recql4* mutations and their corresponding predicted protein products. (C) Breeding data from 49 litters of *Recql4*$^{G522Efs/+}$ and 24 litters of *Recql4*$^{R347X/+}$ intercrosses. Observed and expected mendelian frequencies of the indicated genotypes are shown. No statistical significance was achieved. (D) Western blot of thymocyte lysates from *Recql4*$^{+/+}$, *Recql4*$^{G522Efs/+}$, and *Recql4*$^{R347X/+}$ probed with anti-mouse RECQL4 (clone 3B10; top). The same blot re-probed with anti-Actin (bottom). (E) Western blot of lysates from HoxB8 immortalized *R26*-CreER^{T2} *Recql4*$^{+/+}$ infected with MSCV puro 3xFlag RECQL4 and probed with anti-RECQL4 (clone 3B10; top) and M2 anti-Flag antibody (bottom). (F) Fluorescent microscopy of RECQL4 expression in Kusa 4b10 cells with murine mCherry fused WT, K525A, G522Efs, and R347X and (G) human EGFP fused WT, K508A, C525Efs, and R350Gfs mutations.

Fig. 2. Germline truncating mutants G522Efs and R347X cause low bone mass and narrow bones. (A) Gross body weights of 10-week old male *Recql4*$^{+/+}$, *Recql4*$^{G522Efs/+}$, and *Recql4*$^{R347X/+}$ mice. Micro-CT measurements of (B) Tibial length, (C) Mediolateral width, and (D) Anteroposterior width from 10-week old males *Recql4*$^{+/+}$, *Recql4*$^{K525A/K525A}$, *Recql4*$^{G522Efs/+}$, and *Recql4*$^{R347X/+}$ mice. (E) Trabecular region of interest beginning at 3.5% (Offset) distal to the growth plate and extending for 5% (ROI) of the total tibia length. (F) Trabecular bone volume. (G) Trabecular number. (H) Trabecular separation. (I) Representative images (Axial plane) of reconstructed trabecular bone with color-coded quantitative mineralization from germline *Recql4* mutants. (J) Cortical region of interest beginning at 40% (Offset) distal to the growth plate and extending for 5% (ROI) of the total tibia length. (K)

983 Cortical thickness. (L) Periosteal perimeter. (M) Moment of inertia. (N)
984 Representative images (Axial plane) of reconstructed cortical bone with color-coded
985 quantitative mineralization from germline *Recql4* mutants. Data expressed as mean ±
986 SEM, Ordinary one-way ANOVA. *P<0.05; **P<0.01; ***P<0.001; ****P<0.0001. +/+,
987 n=7; K/K, n=10; G/+, n=6, R/+, n=7. Experiments were independently executed on
988 separate cohorts, with results pooled for presentation. K=K525A; G=G522Efs;
989 R=R347X.
990
991 **Fig. 3. Expression of only the truncating mutations in pre-osteoblasts results**
992 **in low bone mass.** (A) Gross body weights of 10-week old males *Osx*-Cre *Recql4*$^{fl/+}$,
993 *Osx*-Cre *Recql4*$^{fl/K525A}$, *Osx*-Cre *Recql4*$^{fl/G522Efs}$, and *Osx*-Cre *Recql4*$^{fl/R347X}$ mice. (B)
994 Tibial length. (C) Trabecular bone volume. (D) Trabecular number. (E) Trabecular
995 separation. (F) Representative images (Axial plane) of reconstructed trabecular bone
996 with color-coded quantitative mineralization from *Osx*-Cre *Recql4* mutants. (G)
997 Cortical thickness. (H) Periosteal perimeter (I) Moment of inertia. (J) Mediolateral
998 width. (K) Anteroposterior width. (L) Representative images (Axial plane) of
999 reconstructed cortical bone with color-coded quantitative mineralization from *Osx*-Cre
1000 *Recql4* mutants. Data expressed as mean ± SEM, Ordinary one-way ANOVA.
1001 *P<0.05; **P<0.01; ***P<0.001; ****P<0.0001. fl/+, n=9; fl/K, n=6; fl/G, n=7, fl/R, n=7.
1002 Experiments were independently executed on separate cohorts, with results pooled
1003 for presentation. fl=Floxed; K=K525A; G=G522Efs; R=R347X.
1004
1005 **Fig. 4. Compound heterozygous *Recql4* mutants tolerate a sublethal dose of**
1006 **ionizing radiation and do not develop osteosarcoma.** (A) Breeding data from 26
1007 litters of *Recql4*$^{G522/K525A}$ and 25 litters of *Recql4*$^{R347X/K525A}$ intercrosses. Observed and
1008 expected mendelian rates of the indicated genotypes are shown. No statistical
1009 significance was achieved. (B) Kaplan-Meier tumor-free survival plots of the indicated
1010 genotypes. +/+, n=17; K/+, n=39; G/K, n=21; R/K, n=14. (C) Schematic

representation of experimental setup. Compound heterozygous mutants received a single dose of 5-Gy gamma-irradiation, and peripheral blood was assessed, and the animals monitored for tumor formation. Mice were euthanized at the last timepoint. Peripheral blood cell counts following irradiation: (D) Leukocytes; (E) Red blood cells; (F) Platelets; (G) B cells; (H) CD4 T cells; (I) CD8 T cells. (J) Kaplan-Meier tumor-free survival plots of the irradiated mice. K/+, n=5; G/K, n=3; R/K, n=6. Data expressed as mean ± SEM, Ordinary one-way ANOVA. *P<0.05; **P<0.01; ***P<0.001; ****P<0.0001. TBI=Total body irradiation; K=K525A; G=G522Efs; R=R347X.

Fig. 5. Truncating human RECQL4 mutations C525Afs and R350Gfs fail to rescue *Recql4* deletion and impede proliferation, similar to their murine homologs, while mutations that conserve the protein are better tolerated. Proliferation curves of HoxB8 immortalized *R26*-CreER^{T2} myeloid cells without (fl) and with (Δ) tamoxifen-mediated *Recql4* deletion in the following cell lines: (A) fl/+; (B) fl/K525A; (C) fl/G522Efs; (D) fl/R347X. Proliferation curves of HoxB8 immortalized *R26*-CreER^{T2} *Recql4*$^{fl/fl}$ control myeloid cells (E) in the presence or absence of tamoxifen, and EGFP hRECQL4 over-expressing cells: (F) Wild type; (G) K508A; (H) C525Afs; (I) R350Gfs; (J) R807Pfs; (K) Q757X; and (L) L638P. Dotted lines represent individual controls not treated with tamoxifen. (M) Microscopy of EGFP-hRECQL4 expression in HoxB8 cells with WT, K508A, C525Afs, R350Gfs, R807Pfs, Q747X, L638P. A schematic illustration of the expected protein products is outlined below each figure. Orange box represents the Sld2-like region, red box the helicase region. Cell proliferation assays using murine mutations were repeated two times using independent cell lines (replicate plotted supplemental figure S6). Retroviral complementation assays with human constructs were performed two times using the same parental cell line; Data from each replicate are plotted separately.

Molecular and Cellular Biology

A.

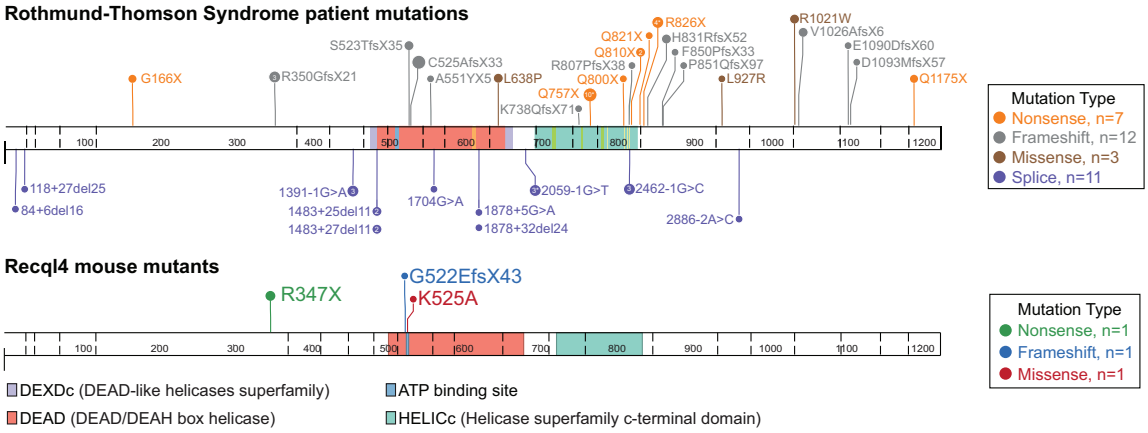

B.

Recql4 Allele	RECQL4 Protein	Protein Size
WT	ATP-binding site; 1, 400, 800, 1200; Sld2; Helicase domain	1216 aa
K525A	K525A; 1, 400, 800, 1200; Sld2; Helicase domain	1216 aa
G522Efs	G522Efs; 1, 400; Sld2	566 aa
R347X	R347X; 1, 200; Sld2	347 aa

C.

Line	Genotype	Observed (%)	Expected (%)
Recql4 G522Efs (From heterozygous intercrosses) 49 Litters	*Recql4* $^{+/+}$	75 (33.8%)	55.5 (25%)
	Recql4 $^{G522Efs/+}$	147 (66.2%)	111 (50%)
	Recql4 $^{G522Efs/G522Efs}$	0 (0%)	55.5 (25%)
Recql4 R347X (From heterozygous intercrosses) 24 Litters	*Recql4* $^{+/+}$	36 (34%)	26.75 (25%)
	Recql4 $^{R347X/+}$	71 (66%)	53.5 (50%)
	Recql4 $^{R347X/R347X}$	0 (0%)	26.75 (25%)

D.

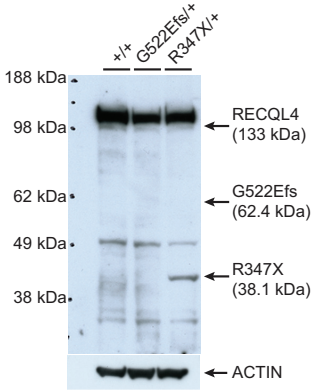

E.

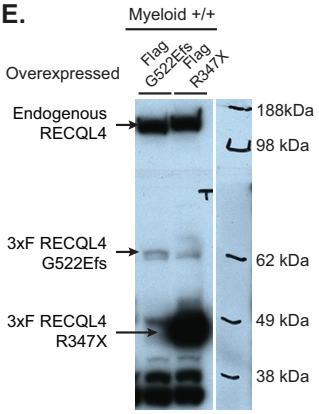

F.

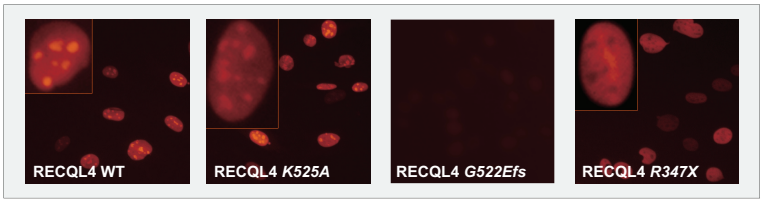

G.

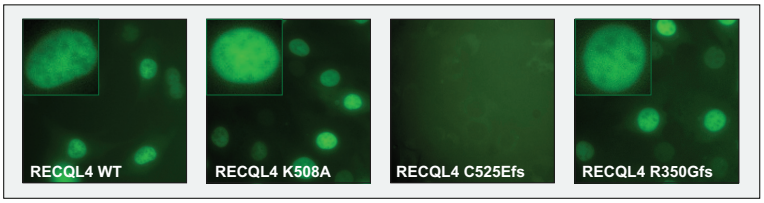

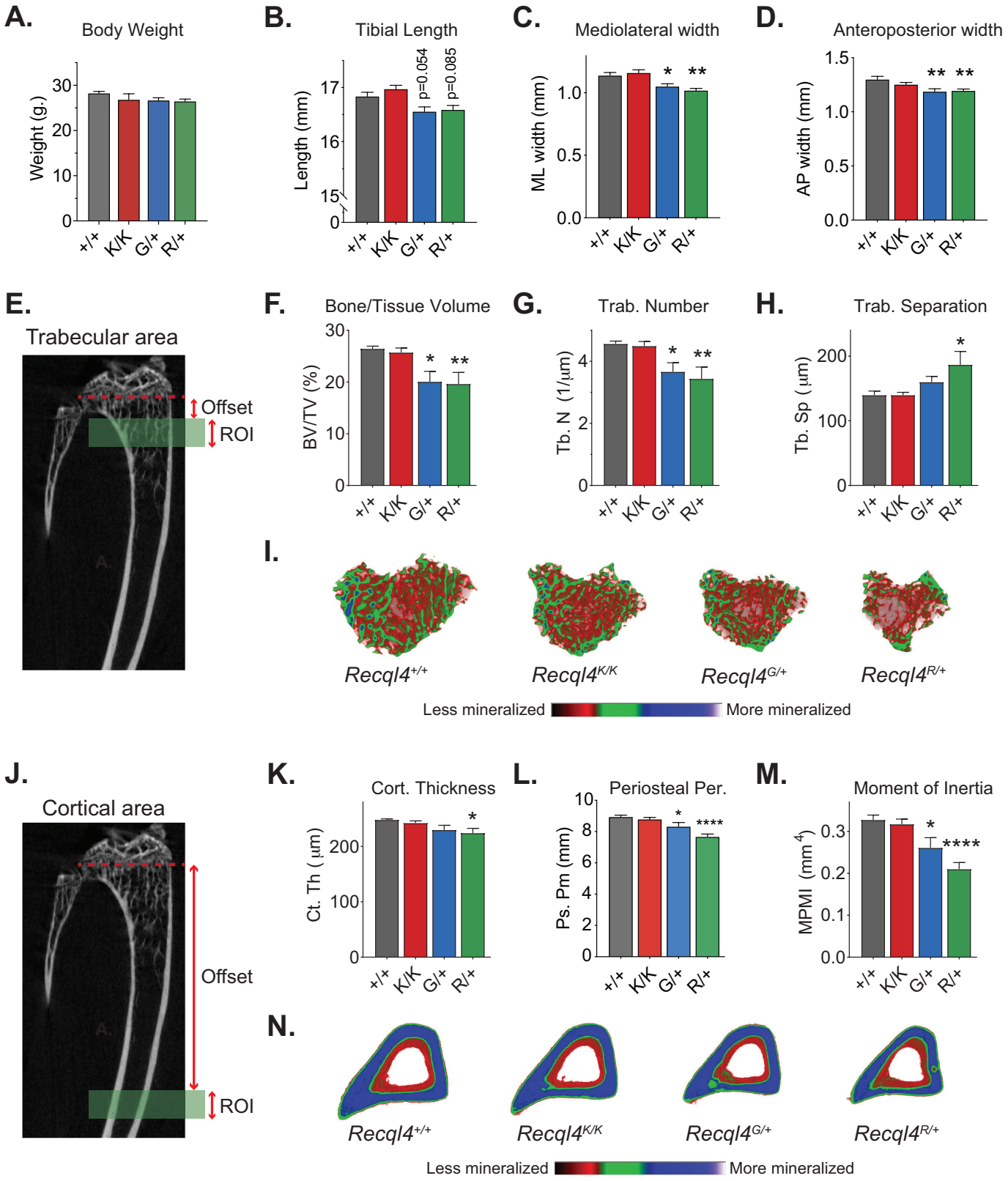

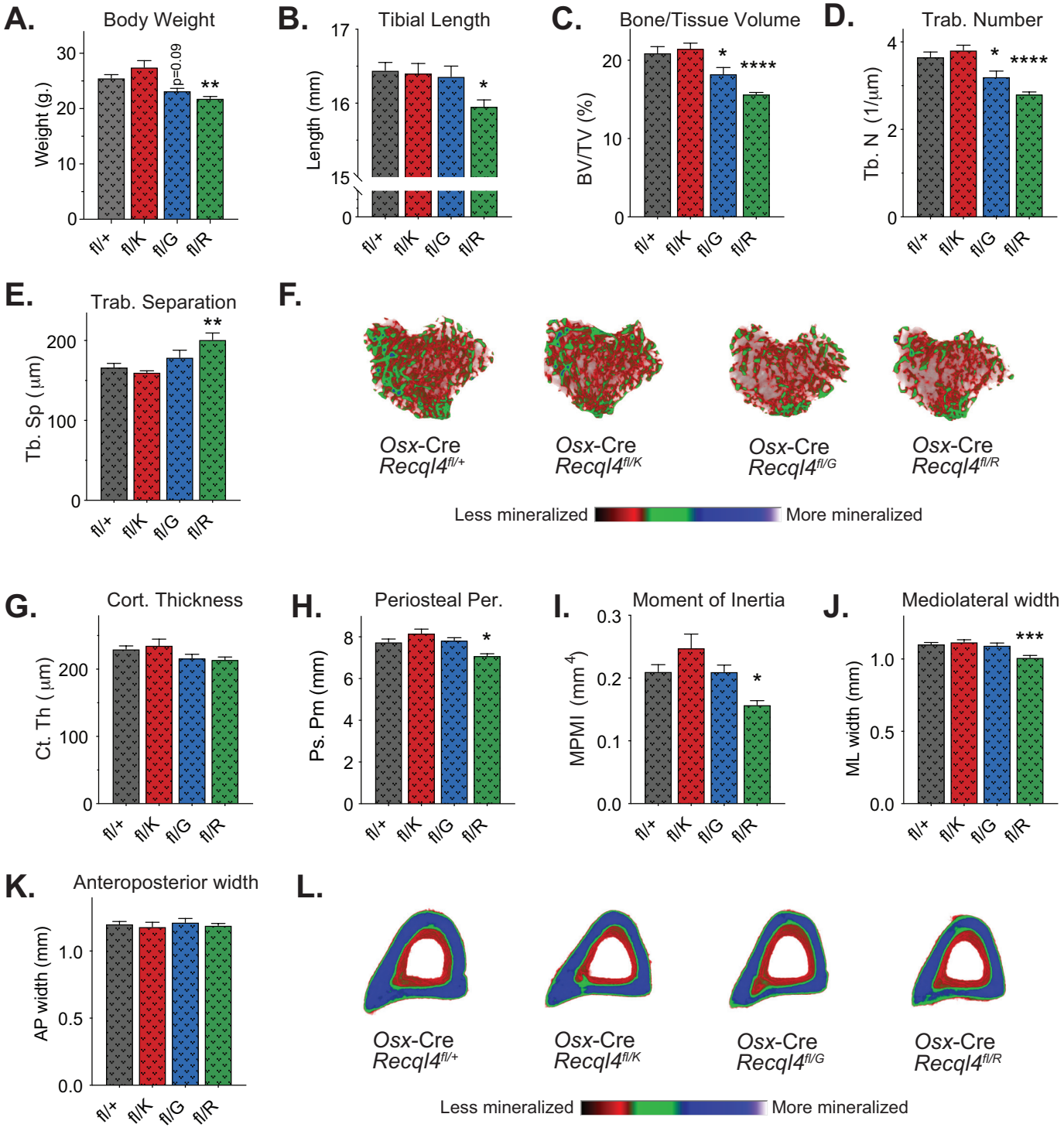

A.

Line	Genotype	Observed (%)	Expected (%)
Recql4 G522Efs/K525A (From hom K525A and het G522Efs) 26 Litters	*Recql4* $^{K525A/+}$	80 (51%)	78 (50%)
	Recql4 $^{G522Efs/K525A}$	76 (49%)	78 (50%)
Recql4 R347X/K525A (From hom K525A and het R347X) 25 Litters	*Recql4* $^{K525A/+}$	67 (52.3%)	64 (50%)
	Recql4 $^{R347X/K525A}$	61 (47.7%)	64 (50%)

B.

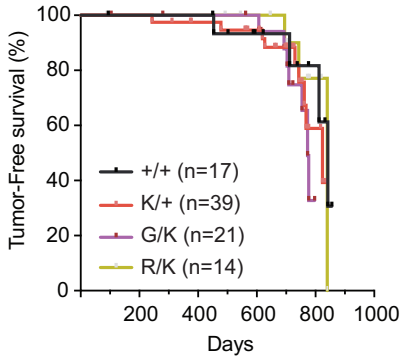

C.

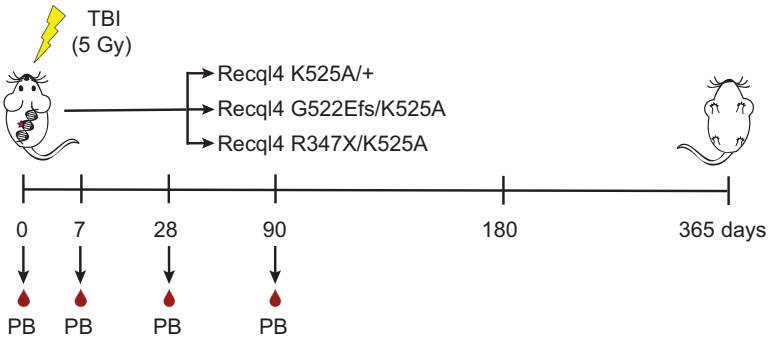

D.

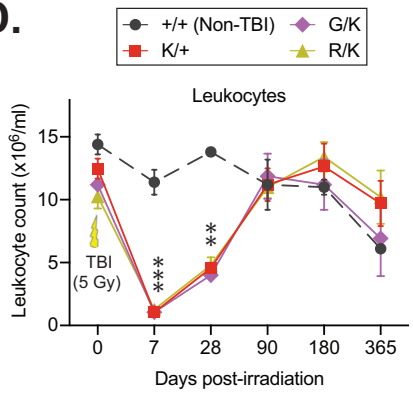

E.

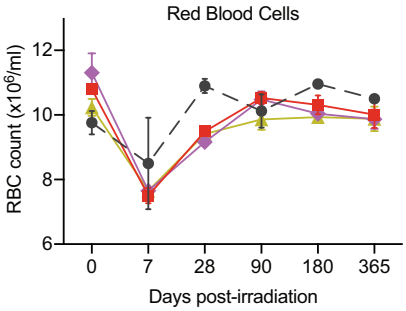

F.

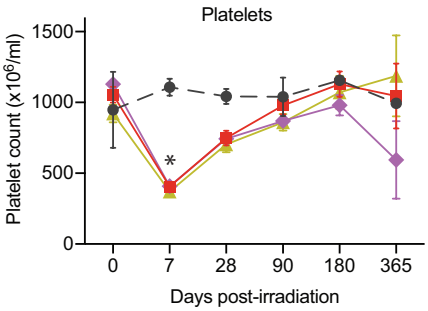

G.

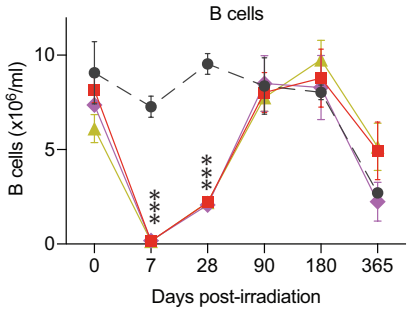

H.

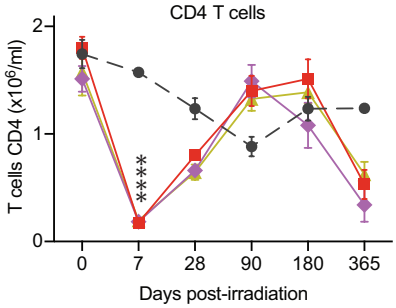

I.

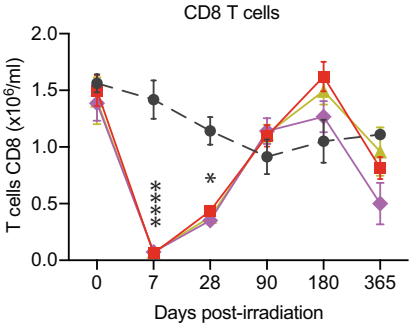

J.